Lasers in Surgery and Medicine 22:193–206 (1998)

Monte Carlo Simulations for EndoBronchial Photodynamic Therapy: The Influence of Variations in Optical and Geometrical Properties and of Realistic and Eccentric Light Sources

Lars H. Murrer, PhD,* Hans P. Marijnissen, PhD, and Willem M. Star, PhD

Department of Radiation Oncology, Subdepartment of Clinical Physics, University Hospital Rotterdam - Daniel Den Hoed Cancer Centre/Dijkzigt Hospital, 3008 AE Rotterdam, The Netherlands

Background and Objective: **Light dosimetry for endobronchial photodynamic therapy is not very advanced to date. This study investigates the dependency of the fluence rate distribution in the bronchial wall on several parameters.**
Study Design/Materials and Methods: **A Monte Carlo model is employed for the illumination of a cylindrical cavity by a linear diffuser to compute the fluence rate distribution in the tissue. The influence of optical and geometrical properties (e.g., the absorption coefficient of the bronchial mucosa and the diameter of the treated lumen) have been investigated, as well as the consequences of varying output characteristics of the diffusers. The optical properties used are those of ex vivo pig bronchial mucosa.**
Results: **With on-axis linear diffusers that can be modelled as a row of isotropic point sources, a constant fluence rate buildup factor can be employed for varying diffuser lengths and lumen diameters. Extreme off-axis placement of the diffuser causes a highly variable, considerable increase in the maximum fluence rate as well as a highly asymmetrical fluence rate profile on the circumference of the illuminated lumen. The fluence rate profiles resulting from illumination with realistic diffusers can be evaluated by implementing the measured radiance profiles of these diffusers in the model. The changes in fluence rate caused by variations in the optical properties of the bronchial mucosa could be accounted for by diffusion theory. This relationship can be used to extrapolate the ex vivo results to the clinical situation.**
Conclusion: **A set of practical rules of thumb is presented that can help to estimate fluence rate distributions in clinical practice. Lasers Surg. Med. 22:193–206, 1998.** **© 1998 Wiley-Liss, Inc.**

Key words: bronchus; light dosimetry

INTRODUCTION

Few studies have been published on the light dosimetry during EndoBronchial Photodynamic Therapy (EB-PDT) [1–3]. These studies show that the light dosimetry in the upper respiratory tract strongly depends on light source positioning, optical properties of the tissue, and the diameter of

Contract grant sponsor: Dutch Cancer Society; Contract grant number: DDHK 93-615.

*Correspondence to: Lars H. Murrer, Department of Radiation Oncology, Subdepartment of Clinical Physics, University Hospital Rotterdam - Daniel Den Hoed Cancer Centre/ Dijkzigt Hospital, P.O. Box 5201, 3008 AE Rotterdam, The Netherlands.

Accepted 2 February 1998

the lumen that is illuminated. We showed that the fluence rate distribution calculated with Monte Carlo simulations provides accurate absolute values for the fluence rate as measured ex vivo in a pig trachea [1].

Monte Carlo simulations offer the possibility to vary the geometry and optical properties [4] to assess the influence of those parameters on the fluence rate distribution. Especially in complex geometries where analytical radiative transport calculations are not feasible, the Monte Carlo simulations prove particularly useful to achieve more insight (qualitatively as well as quantitatively) in the role of geometry and optical properties.

The present work describes the fluence rate distributions as a result of different illumination conditions and interrelates the different conditions by rules of thumb. In this way the fluence rate distribution calculated in the ex vivo pig trachea can be used to make estimates in the clinical situation. The issues addressed are the influence of the length and emission profile of the light source, the on- or off-axis positioning of the light source, the diameter of the treated lumen, and the influence of the optical properties on the fluence rate buildup.

MATERIALS AND METHODS

Monte Carlo Model

The Monte Carlo code was adapted from the Pascal code used to simulate whole bladder wall illumination [5,6]. The simulations were run on a Pentium PC. The geometry of the experiment was modelled as a cylinder of air (diameter D) embedded in a cylindrically symmetric semi-infinite medium (thickness T, outer radius $r \rightarrow \infty$) (Fig. 1). T was chosen 5 cm, which was the length of the trachea specimens used in previous experiments [1]. Making the slab thicker generally resulted in no significant changes in light distribution, and for the sake of spatial resolution, the slab thickness was kept limited. The air in the cylinder has negligible absorption and scattering, and the index of refraction is 1.

The semi-infinite medium has the optical properties of the mucosa layer at the inner side of the trachea at the chosen wavelength (λ = 630 or 514 nm). The optical properties $\mu_a(cm^{-1})$ the absorption coefficient, $\mu_s(cm^{-1})$ the scattering coefficient and g(–) the anisotropy coefficient for the mucosa of pig tracheas were measured ex vivo with a double-integrating sphere setup combined with an Inverse Adding Doubling (IAD) algorithm [7]. The average values (630 nm, n = 6; 514 nm, n = 4) as well as the value for one individual trachea (630 nm) that were used in the simulations are shown in Table 1. The refractive index of the mucosa is 1.37 (±0.01) for the wavelengths used [1].

The linear light source with a length L is modelled as a continuous distribution of isotropic and equally strong point sources or with strength varying with position and anisotropic radiance (see below). The quality of linear diffusers available now is such that they can be accurately described with isotropic point sources [8]. The diffusers simulated in this work will consist of equally strong and isotropic point sources, unless otherwise stated. The light source was placed either on the central axis or eccentrically with a distance x from the central axis. In the case of central placement of the light source, a two-dimensional grid was employed to store the data. In the case of off-axis placement of the light source the cylindrical symmetry is violated and a three-dimensional grid was employed. In the 3D case, more photons (N ≈ 250,000) were needed to obtain a good signal-to-noise ratio, as opposed to the 2D case where only one-tenth of this number (N ≈ 25,000) was required. Several runs were performed (N = 3.5) to calculate the standard deviations on the simulated values for the fluence rate. The resolution in the z, r, and ϕ direction was 1 mm, 0.2 mm, and 6°, respectively.

Theoretical Considerations for Cylindrical Symmetry

The geometry parameter Q is defined as:

$$Q = L/D \tag{1}$$

With L (cm) the length of the diffuser and D (cm) the diameter of the lumen. The incident fluence rate (mW/cm^2) at a certain point is defined as the fluence rate in air at that point as a result of the light emitted by the diffuser, without contributions of backscattering by the tissue. The incident fluence rate on the wall of the cavity calculated from a radially emitting (perpendicularly to the diffuser's axis) line source is:

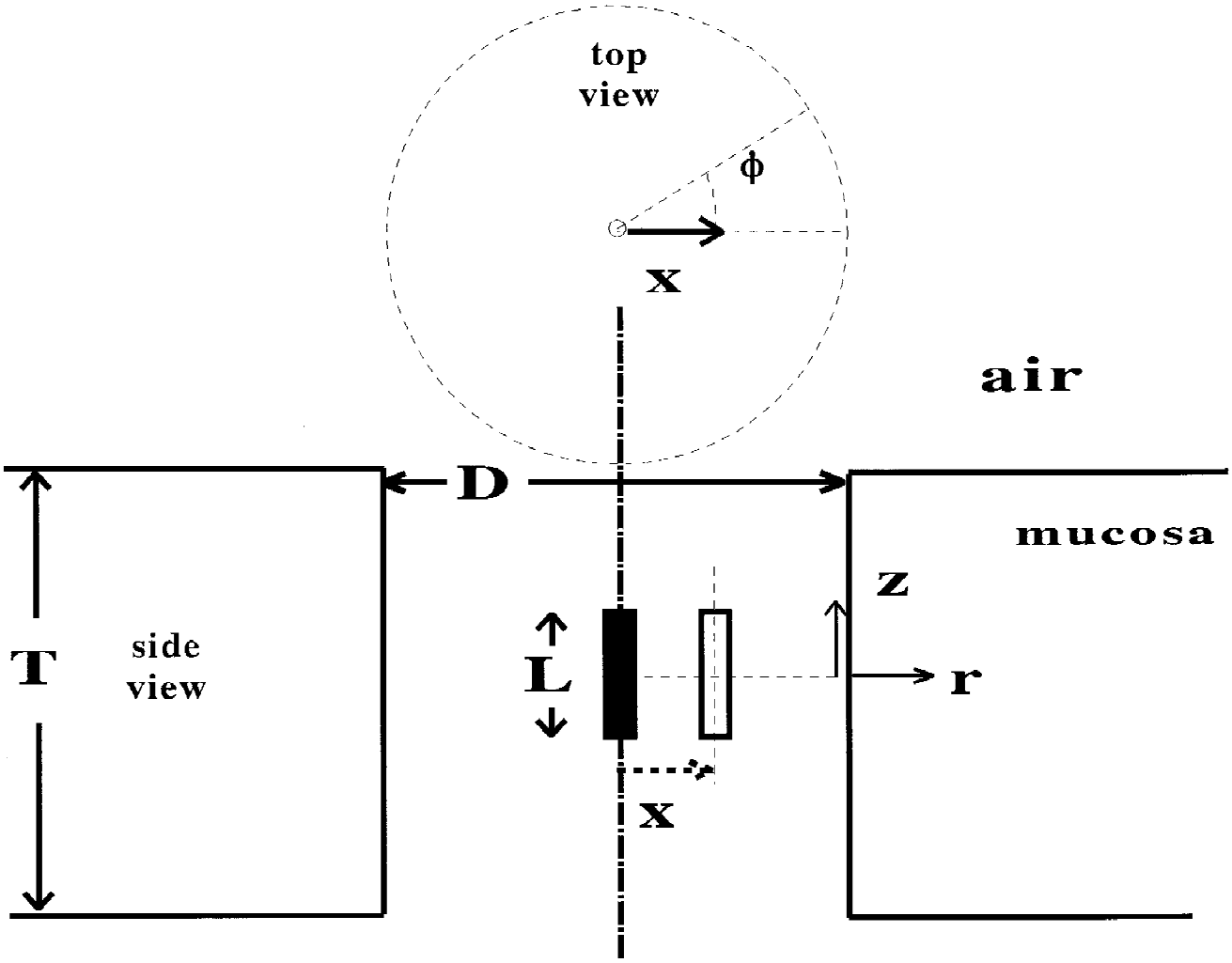

Fig. 1. Monte Carlo model geometry, with L the length of the diffuser, D the diameter of the cavity, T the thickness of the slab, x the eccentricity of the light source, r the depth in the tissue, and z the height, ϕ azimuthal angle.

TABLE I. Optical Properties of Bronchial Mucosa*

Wavelength (nm)	Absorption μ_a (cm^{-1})	Scattering μ_s (cm^{-1})	Anisotropy g (–)	Remark
630	0.22 (0.17)	113 (19)	0.80 (0.06)	n = 6
630	0.15 (0.02)	81.2 (0.9)	0.77 (0.01)	single trachea
514	1.83 (1.01)	119 (19)	0.77 (0.08)	n = 4

*Measured ex vivo with a double-integrating sphere setup. The data on 630 nm were published before [1], the 514 nm data are similar to those found by Van Staveren et al. [6] for bladder mucosa. Standard deviations between parentheses.

$$\phi_{inc,radial}(z) = \begin{cases} P/(\pi LD) & \leftarrow |z| \leq L/2 \\ 0 & \leftarrow |z| > L/2 \end{cases} \quad (2)$$

with P (mW) the total output power of the diffuser and z (cm) the position on the wall relative to the middle of the diffuser (Fig. 1). This source function does not describe the actual situation, but is sometimes used as a rough estimate by dividing the output of the diffuser by the estimated area of illumination (the surface area of a cylinder with radius D and length L).

If, more realistically, a superposition of isotropic point sources is considered as a model for the linear diffuser, the incident fluence rate on the wall (mW/cm^2) is described by:

$$\phi_{inc,isotropic}(z) = \frac{P}{\pi LD}\frac{1}{2}\left(\arctan\left[\frac{L-2z}{D}\right]\right.$$

$$+ \arctan\left[\frac{L + 2z}{D}\right]\Bigg), \qquad (3)$$

which is equation 2 corrected by a factor describing the geometry.

In the case of isotropic point sources, the ratio R between the incident fluence rate at $z = \pm L/2$ and $z = 0$ (opposite middle and endings of the diffuser, respectively) yields:

$$R = \frac{\phi_{inc}(z = \pm L/2)}{\phi_{inc}(z = 0)} = \frac{\arctan[2Q]}{2 \arctan[Q]} \qquad (4)$$

The fluence rate buildup factor β is defined as the ratio of the incident fluence rate on the cavity wall at $z = 0$ divided by the measured (or simulated) fluence rate at the position ($\phi_{true}(z = 0)$) in the case of on-axis position of the diffuser (1).

$$\beta = \frac{\phi_{true}(z = 0)}{\phi_{inc}(z = 0)} \qquad (5)$$

For the two different source terms (radial and diffuse) β is:

$$\beta_{radial} = \frac{\pi LD}{P} \phi_{true,radial}(z = 0) \qquad (6)$$

and

$$\beta_{isotropic} = \frac{\pi LD}{P} \frac{\phi_{true,isotropic}(z = 0)}{\arctan[Q]} \qquad (7)$$

The expression for β derived from diffusion theory [9] for an infinitely long, radially radiating, diffuser in an infinitely long cylindrical (air)cavity in an infinite medium yields:

$$\beta_{dif\ f.th.} = \frac{\mu_{eff}}{\mu_a} - 2 \qquad (8)$$

with μ_{eff} (cm^{-1}) the effective attenuation coefficient, defined as: $\mu_{eff} = \sqrt{3\mu_a(\mu_a + (1 - g)\mu_s)}$.

Realistic Light Sources

Using a uniformly distributed random variable, the distribution of the site and elevation angle of emission θ of the photons from the linear diffuser is generated for Monte Carlo simulations (see Appendix). The azimuthal angle ϕ is taken randomly from the interval $[0,2\pi]$. The distribution of the place of emission is described by the total probability of light emission at each position of the diffuser, estimated by summing the radiance in all directions at that position. The measurement of these profiles was described in detail by Murrer et al. [10]. Furthermore, the angular distribution of the light emitted from the diffuser at a particular position on the diffuser is generated. Here, the distribution of the emission angle of the photon is described by a 6^{th} degree interpolation polynomial as described by Murrer et al. [10]. The diffuser used as an example in [10] is used again here.

In Figure 2, a comparison is made between the original distribution and the random number generator counts when the above procedure is applied. An example for both the place and the angle of emission is shown. The power distribution of this particular diffuser shows a peak near the end, which is caused by reflections off the end-mirror in this diffuser. The angular distribution of the radiance shows a forward directed pattern (maximum at 30°). The angle indicated is the angle between the direction of the light entering the diffuser and the light emitted by the diffuser. Because of the cylindrical symmetry around the diffuser axis a two-dimensional simulation can be applied.

RESULTS

Radial Vs. Isotropic Source Terms

Figure 3 presents the fluence rate profiles generated by an on-axis linear diffuser that consists of either radially or isotropically radiating elements. A 2 cm diffuser in a cavity of 2 cm diameter was simulated, and the average optical properties for 630 nm (Table 1) for the mucosa were used. The resulting fluence rates at $z = 0$ and $r = 0$ are 680(12)—standard deviations between parentheses—mW/cm^2 (radial) and 487(16) mW/cm^2 (isotropic). The calculated incident fluence rates (see Materials and Methods) are 79.6 (radial) and 62.5 mW/cm^2 (isotropic), corresponding with β values of 8.5(0.2) and 7.8(0.3), respectively. The depth profiles at $z = 0$ differ only a by constant factor of 1.47(0.02) (average of all depths), and both reach the level of the incident fluence rate at 5 mm depth. The rectangular radial incident fluence rate pattern as indicated in Figure 3 causes a fluence rate pattern on the cavity wall that is much narrower than the profile caused by the bell-shape incident fluence rate pro-

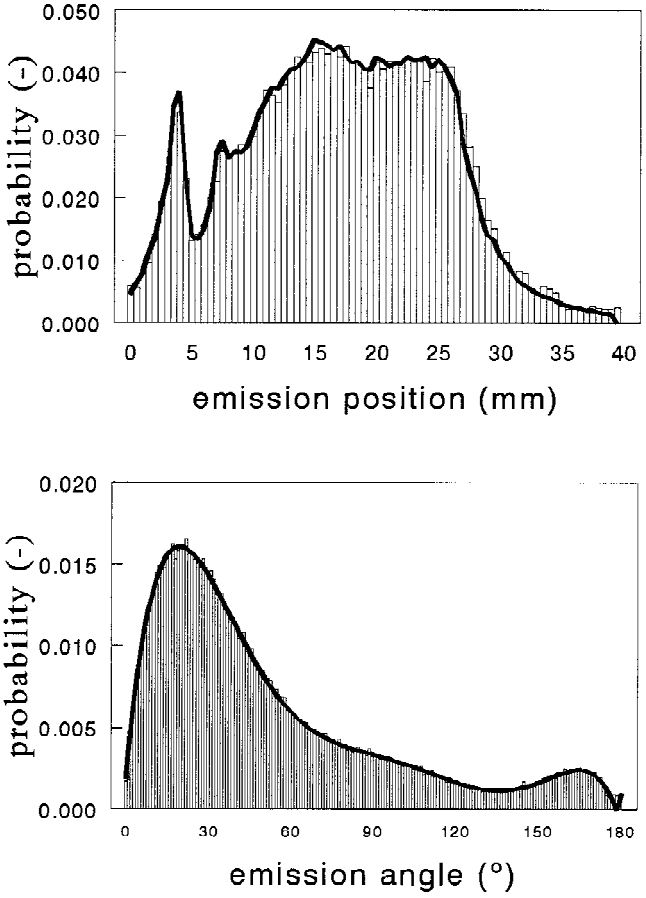

Fig. 2. Random number distributions describing the probability distribution of the site of emission (top) and the elevation angle θ of emission (bottom) (on position 15 mm) of the linear diffuser. The bars represent the counts of the random number generator per bin, the solid lines represent the measured distributions.

file of the isotropic source. The resulting radial profile reaches 10% of the maximum value at 13 mm from the center, whereas the isotropic profile reaches this level at 24 mm from the center.

Nonideal Light Source

In Figure 4, the fluence rate profile on the wall of the trachea as simulated with the measured source characteristics (see Materials and Methods) placed on-axis is compared with the profile measured in an ex vivo pig trachea with unknown optical properties. For the simulations, the average optical properties for $\lambda = 630$ nm are used (Table 1). Although the profiles for measurement and simulation do not coincide, the figure shows that the position of the maximum of the fluence rate on the wall is the same (within measurement and simulation accuracy) for both curves. The calculated (2.1 mW/cm^2) and measured (2.8 mW/cm^2) fluence rates at the maximum are of the same order of magnitude, but do not agree within error ranges. This is to be expected, because the simulation uses optical properties different from those of the measured trachea. However, the distinct asymmetry in the measured profile is reproduced in the simulation.

Variations in L and D: The Geometry Parameter

In Figure 5, the $\beta_{\text{radial-estimate}}$ and $\beta_{\text{isotropic}}$ values are shown, calculated from the simulated value for ϕ_{true}, using both the incorrect, estimated radial source function $\phi_{\text{inc,radial}}$ and the correct isotropic $\phi_{\text{inc,isotropic}}$ source function. The relationship $\beta_{\text{isotropic}} = \beta_{\text{radial-estimate}}/\arctan[Q]$ connects the two β-values. The β-values are plotted as a function of the geometry parameter Q for both 630 and 514 nm light.

The values of L and D were varied from 1–5 cm in steps of 1 cm. The figure shows that the geometry parameter is useful to describe β in different geometries. In the left part of the figure, the β values calculated with the incorrect (roughly estimated) radial source function show a one-to-one correspondence between β and the geometry parameter. When the correct source term is used to calculate the β value (right part), β is almost constant with a slow decrease with increasing values of Q. A linear curve-fit yields: $\beta_{630}(Q) = 8.36 - 0.34Q$ ($r = 0.78$) and $\beta_{514}(Q) = 3.32 - 0.15Q$ ($r = 0.83$) with r the correlation coefficient. A first-order estimate of β for all geometries can be made by taking the average value of β for all values of the geometry parameter, which is 7.7(±11%) for 630 nm and 3.0(±11%) for 514 nm. The slow decrease of β with increasing Q is probably caused by the finite length of the cylindrical cavity. High Q values occur for long diffusers (4 and 5 cm) in the set of L and D values that were simulated. These diffusers lose relatively much light out of the ends of the cavity because their lengths are close to the thickness of the slab ($T = 5$ cm).

The fluence rate at $z = \pm L/2$ and $r = 0$ (opposite the ends of the diffuser) can be estimated roughly using eq. (4), assuming that the shape of the total fluence rate profile does not differ too much from the incident profile. The fluence rate is then estimated by taking the fluence rate at $z = 0$, and multiplying it by the factor of eq. (4). The simulated fluence rate is 86%(22) of the value estimated for 630 nm and 90%(16) for 514 nm. This indicates that, on average, the total fluence rate

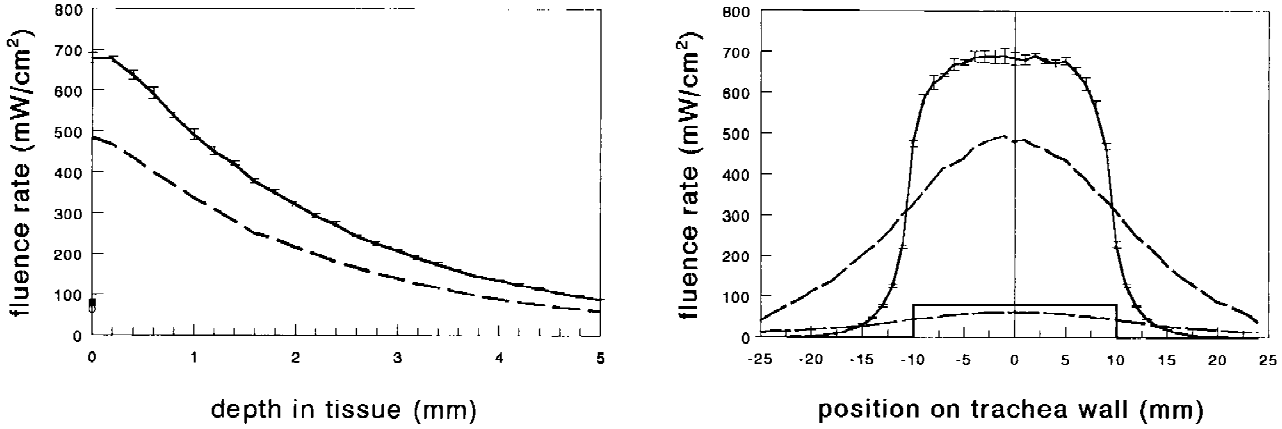

Fig. 3. Fluence rate profiles resulting from illumination by a 2 cm diffuser (total output of 1,000 mW) with both radial (solid lines) and isotropic (dashed lines) emission patterns. Diameter of the cavity is 2 cm, optical properties: average values for 630 nm (Table 1). Error bars calculated from 5 simulations of 25,000 photons each. For clarity, error bars only on radial curves. Left: fluence rate in tissue at z = 0. Incident fluence rate for radial and isotropic source function indicated by solid and open square, respectively. Right: fluence rate at the wall (r = 0). Incident fluence rate profiles for both source terms are also indicated on the bottom of the graph (solid and dashed lines for radial and isotropic emission patterns, respectively).

profile is somewhat narrower than the incident profile.

Varying Lumen Diameter

In Figure 6 the fluence rate at z = 0 and r = 0, 2 and 5 mm is plotted for varying lumen diameter. The light source is 2 cm long, on-axis, and consisting of isotropic point sources with a total output of 1,000 mW. The average optical properties for 630 nm are used (Table 1). The absolute value of the fluence rate on the wall (e.g., at z = 0) decreases with increasing value of D, as the power emitted by the linear diffuser is distributed over a cylinder with a larger surface area.

The curves for 0 mm, 2 mm, and 5 mm depth in tissue differ only by a constant multiplication factor, which means that the penetration depth (when related to the fluence rate at 0 mm depth) is the same for all lumen diameters. The fluence rate at 2 mm and 5 mm is 41(2)% and 11(1)% of the fluence rate at 0 mm. The average β value for all lumen diameters is 7.2(0.5), in agreement with Figure 5 (same optical properties). The regression line is given by: $\beta_{630}(Q) = 8.21 - 0.53Q$ (r = 0.94).

Variation in Optical Properties: Relation With Diffusion Theory

When the optical properties for the individual trachea (Table 1) are used, the value for $\beta_{diff.th.}$ is 17.3. A Monte Carlo simulation that uses these optical properties and an (isotropic) diffuser of 2 cm (on-axis) in a lumen with a diameter of 2 cm yields a $\beta_{m.c.}$ of 8.4 (±5%). The reason for this difference is that the diffusion theory formula is derived for a different geometry (see Materials and Methods). In order to investigate if the diffusion theory formula can qualitatively describe the dependence of β on the optical properties, the values for both $\beta_{m.c.}$ and $\beta_{diff.th.}$ were normalised by setting them at unity at this set of optical properties. From there, the values for both μ_a and μ_s were varied in the Monte Carlo simulations and the diffusion theory formula. The results are presented in Figure 7.

The normalised β values for varying scattering found for both Monte Carlo and diffusion theory agree well (mean deviation 2%). For varying absorption (μ_a), the agreement is less good. For increasing μ_a, the agreement is still acceptable (mean deviation 15%), but for decreasing μ_a, the discrepancy increases (mean deviation 32%), as is clear from the figure.

The Monte Carlo data show less increase in β with decreasing absorption than diffusion theory. With lower absorption, the photons travel along optical paths that penetrate deeper in the tissue. Because of the finite length of the simulated cavity, photons escape and cause less buildup of fluence rate compared with the infinitely extended diffusion theory geometry.

The variations in μ_s cause changes in β from a decrease of 34% at 40 cm^{-1} to an increase of 26% at 120 cm^{-1}. When μ_a is decreased to 0.05 cm^{-1}, the β value increases by 65%. Increasing the μ_a to

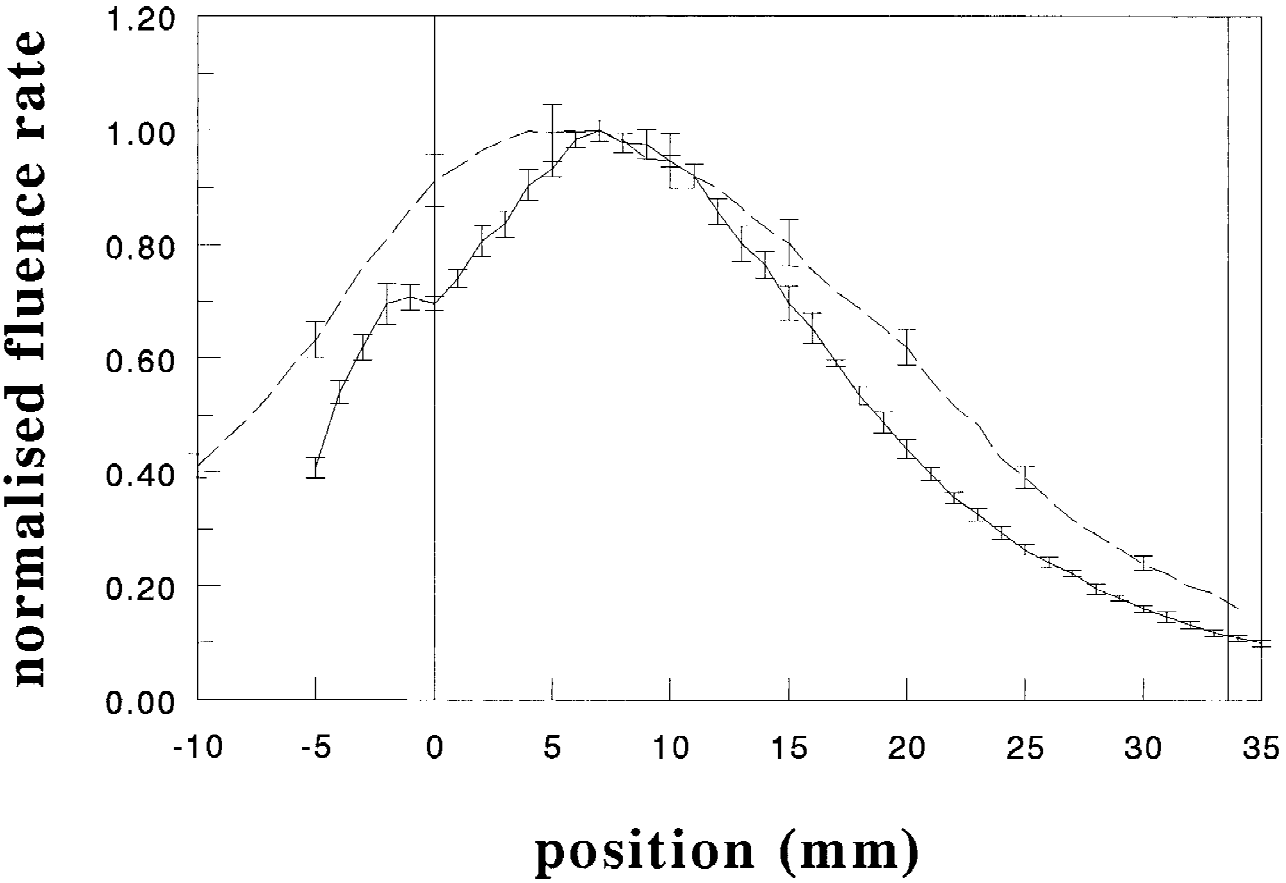

Fig. 4. Fluence rate profile on the wall of an ex vivo pig trachea with a diameter of 19 mm. The length of the diffuser is 3.4 cm, the total output power is 3.4 mWatt. Vertical lines denote the beginning and ending of the diffusing part. Dashed line: as measured with an isotopic probe (taken from Murrer et al. 1995), solid line: Monte Carlo simulation, average of 5 runs of 25000 photons each, average optical properties at 630 nm; see Table 1. Both curves are normalised to the maximum value, located at 8 mm for the measurement (2.8 mW/cm^2) and at 7 mm for the simulation (2.1 mW/cm^2).

0.30 cm^{-1} decreases β by 30%. Variations in μ_a may be expected when the blood content of the tissue changes.

The β values found for 514 and 630 nm light in the section about the geometry parameter can be interrelated with diffusion theory in the above manner. The ratio of $\beta_{\text{diff.th.},630}(= 15.6)$ and $\beta_{\text{diff.th.},514}(= 4.92)$ is 3.2, whereas this ratio for $\beta_{\text{m.c.},630}$ and $\beta_{\text{m.c.},514}$ is 2.6 (0.6). These ratios agree within simulation error.

Also, the above procedure can be used to estimate the unknown absorption coefficient of the pig trachea in which the fluence rate profile resulting from a realistic light source was measured. The simulation with $\mu_a = 0.22$ cm^{-1} resulted in a maximum fluence rate that was 75% of the measured value. Assuming constant scattering properties, the above procedure yields a μ_a of 0.13 cm^{-1} for the trachea, which is a realistic value considering the average value in Table 1.

Eccentric Light Sources

The optical properties of the single trachea (Table 1) were used to investigate the influence of the off-axis placement of the light source. A trachea with D = 2 cm with a diffuser (output 1,000 mW) of 2 cm length was simulated. The resulting fluence rate at z = 0, r = 0 and $\phi = 0°$ and 180° is shown in Figure 8. When the diffuser is placed on-axis, the fluence rate is 548(27) mW/cm^2, corresponding to a β of 8.8(0.4). Moving the diffuser away from the center to the wall increases the fluence rate to 1174(57) mW/cm^2 at 5 mm and 6,110(130) mW/cm^2 at 9.9 mm off-axis, which is a 2- and 11-fold increase of the fluence rate, respectively. The positioning of the diffuser close to the

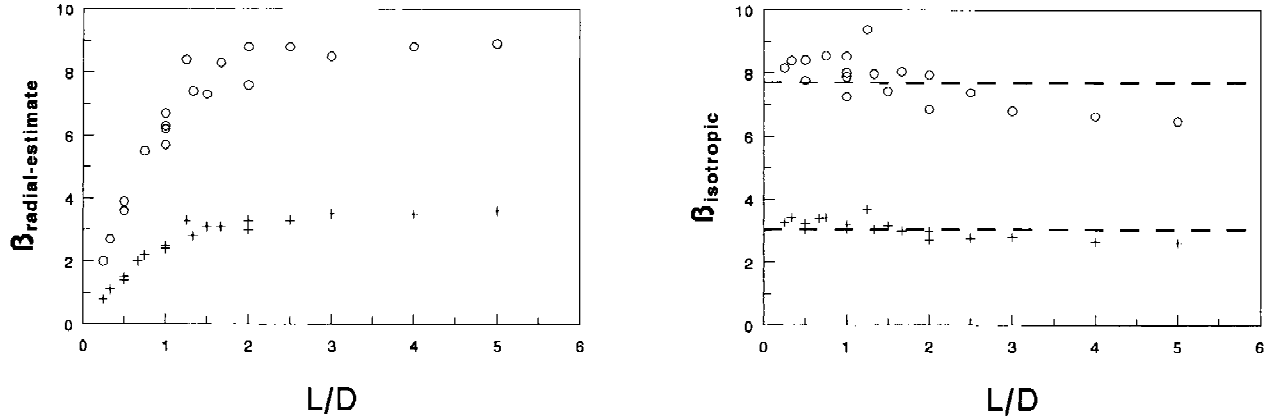

Fig. 5. Monte Carlo simulations of β for varying diffuser lengths and lumen diameters plotted against the geometry parameter. Optical properties are the average for 630 nm (Table 1). Each point is calculated by one run of 25,000 photons, the statistical standard deviation of these values is ≈7%. Left: $\beta_{\text{radial-estimate}}$ for (incorrect) assumption of radially emitting source, Right: $\beta_{\text{isotropic}}$ for correct light source consisting of isotropic point sources. +: λ = 514 nm, ○: λ = 630 nm. The dashed lines indicate the average values of $\beta_{\text{isotropic}}$, 7.7 (sd 0.8) and 3.0 (sd 0.3) for 630 and 514 nm, respectively.

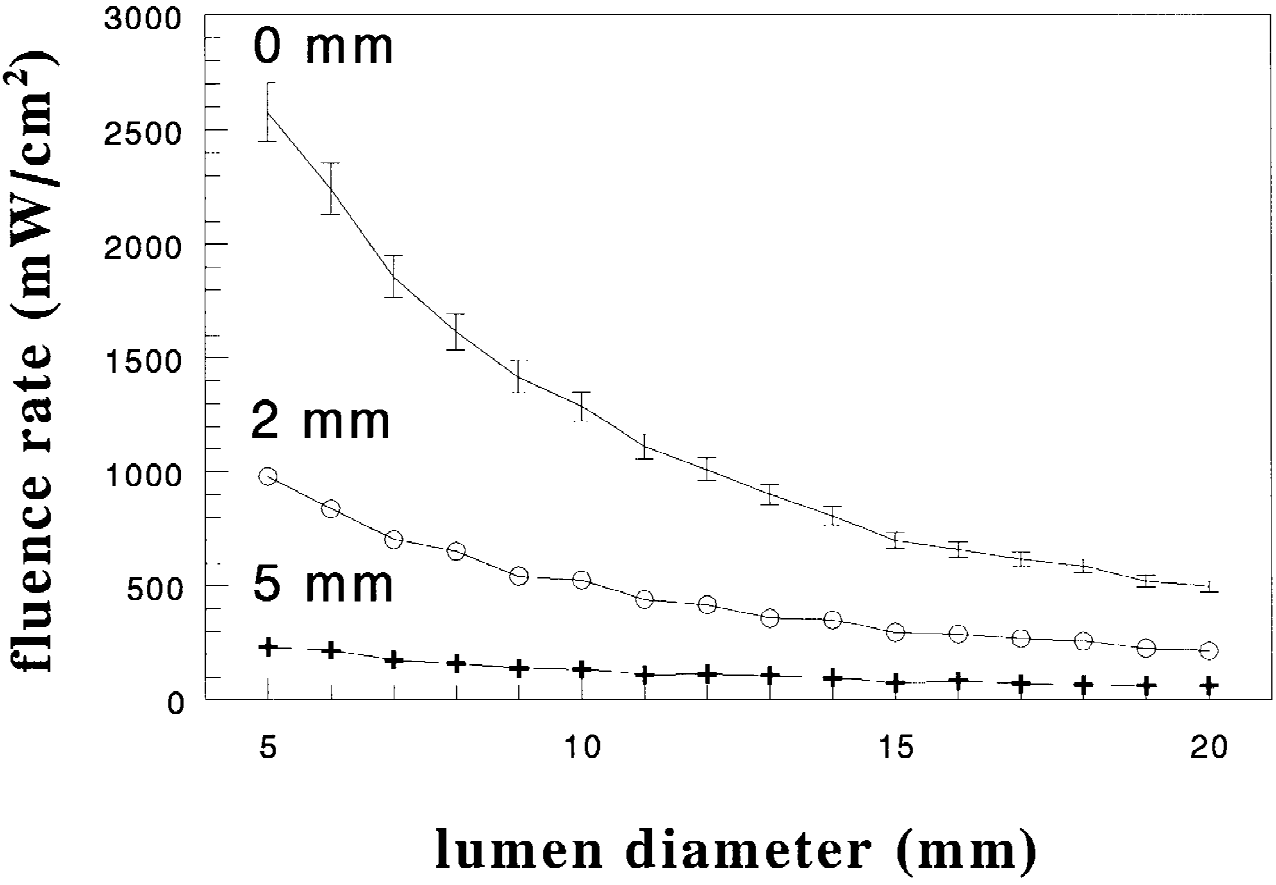

Fig. 6. Fluence rate at z = 0 mm and r = 0, 2 and 5 mm depth in tissue for varying lumen diameter. The simulated (on-axis) diffuser has a length of 2 cm, and a total output power of 1,000 mW. Optical properties are the average values for 630 nm (see Table 1). Mean values and error bars calculated from 5 runs of 25,000 photons each.

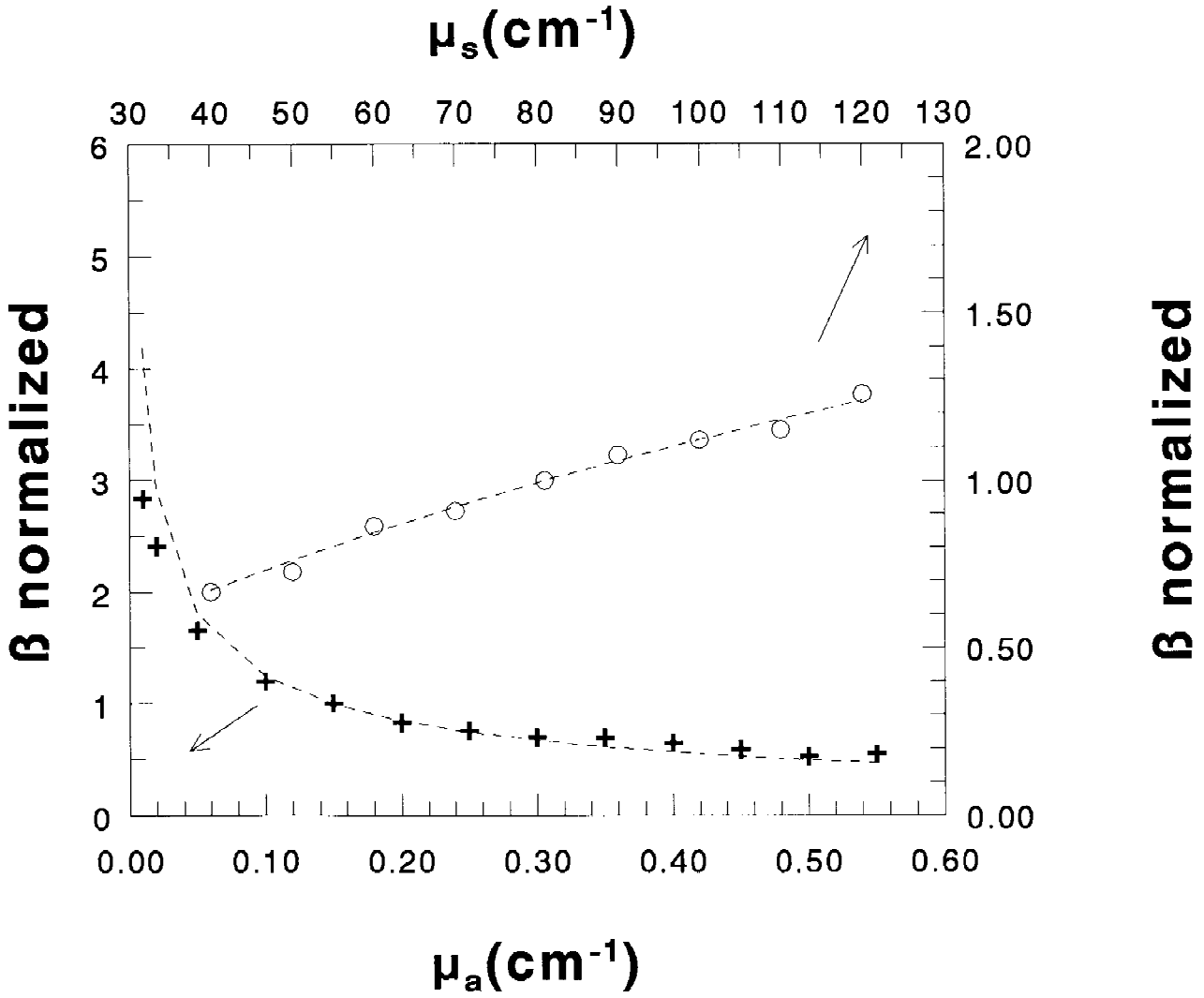

Fig. 7. Variations in β values from diffusion theory (dashed lines) and Monte Carlo simulations (symbols) when μ_a (+, bottom x-axis and left y-axis) or μ_s (○, top x-axis and right y-axis) are varied. The β values are normalised to the β values for diffusion theory and Monte Carlo at $\mu_a = 0.15$ cm^{-1}, $\mu_s = 81$ cm^{-1} and $g = 0.77$. Statistical variations on the Monte Carlo data: ≈7%.

wall is critical for the fluence rate. Moving the diffuser to 9 mm off-axis decreases the fluence rate by 41% to 3,602 mW/cm^2. Moving the diffuser 1 mm off-axis to either side causes a 10% change in the fluence rate. The fluence rate at 180° gradually decreases with increasing off-axis position to a value of 169(10) mW/cm^2 at 9.9 mm off-axis placement. This is 31% of the on-axis level, and 3% of the level at 0°.

Figure 9 presents the fluence rate profiles on the wall of the cavity (r = 0) in the z- and the ϕ-direction. The closer the light source is positioned to the wall, the narrower the profile in the z-direction (top) becomes, which is a consequence of the fact that the incident fluence rate pattern is also narrower, because the diffuse light has less distance to expand before hitting the wall. Figure 9 shows that the relative increase between different off-axis positions is larger for positions close to the surface (cf. 9 and 9.9 mm) as compared to those far away from the surface (cf. –9 and –9.9 mm). This indicates that the fluence rate for off-axis light source positions close to the surface is relatively sensitive to small displacements of the light source.

The profiles in the ϕ direction (bottom) show that profiles narrow considerably for extreme off-axis positions. In the ϕ direction, we define the area of treatment for different off-axis positions as that area with a fluence rate of >50% (arbitrary) of the maximum. For 5 mm, 9 mm, and 9.9 mm off-axis, this area is 23.0 mm, 6.2 mm, and 3.1 mm, respectively.

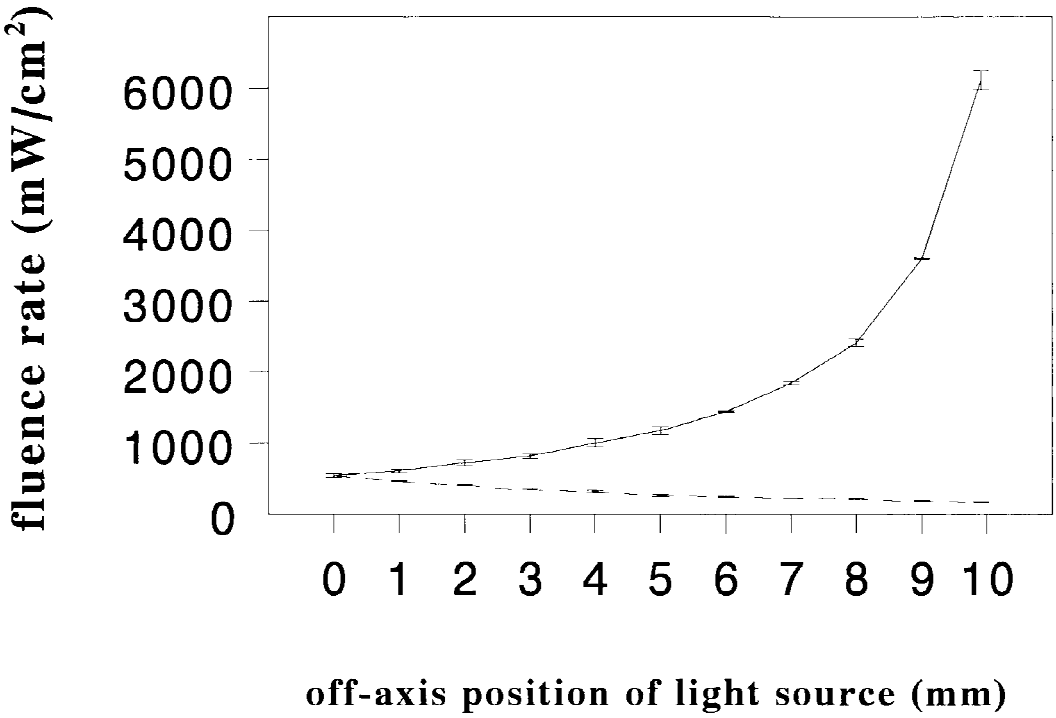

Fig. 8. Fluence rate on z = 0 and r = 0 resulting from illumination of a cavity (D = 2 cm) with an off-axis isotropic diffuser of 2 cm length, optical properties of single trachea (Table 1). Total output power of the diffuser is 1,000 mW. Solid line indicates the fluence rate at $\phi = 0°$, dashed line indicates the fluence rate at the opposite side ($\phi = 180°$). Mean values and error bars calculated of 3 runs of 250,000 photons each.

DISCUSSION

Monte Carlo Model

Although the model of the trachea is simple, we showed previously [1] that it is suitable to simulate absolute values of the fluence rate in the bronchial mucosa (thickness ≈ 1 mm) and to a certain extent in the cartilage (≈3 mm) by use of the optical properties of the mucosa only. This is because the absorption and reduced scattering of the cartilage [1] are very similar to those of the mucosa at 630 nm. With the use of green light, the penetration depth is such that in practice only the mucosa layer needs to be considered in the model. The incorporation of realistic light sources in the model facilitates the interpretation of the consequences of the use of light sources with varying output characteristics. In the future we hope to expand the model with a multilayer structure to incorporate the cartilage and with local spots of different optical properties to simulate lesions.

Source Term

In practice, often a first estimate of the fluence rate on the wall is made by dividing the total output of the diffuser by the surface of the cylinder with the radius of the lumen and the length of the diffuser. This incident fluence rate cannot be used for interpatient comparison, as the fluence rate buildup is highly variable between patients. Another aspect of the above estimate is the underlying assumption of a radially emitting diffuser. The incident fluence rate profile of a real (isotropic) diffuser is not rectangular but bell-shaped. Therefore, a larger margin around the lesion should be illuminated to ensure proper treatment of the tumour and the tumour bed.

Influence of Optical Properties

The analogy between the β values calculated with diffusion theory and those found with Monte Carlo can be used to estimate the variations in β that can be expected when the interspecimen variations in the average optical properties for 630 nm in Table 1 are taken into account. The largest change in β occurs when μ_a and g are lowered by one standard deviation and μ_s increased by one standard deviation (maximum reduced scattering). The β for the average optical properties (7.7, Fig. 5) then increases by a factor of 2.8 to a value of 21.3. The lowest β is 4.0 (52%), for maximum absorption and minimal reduced scattering.

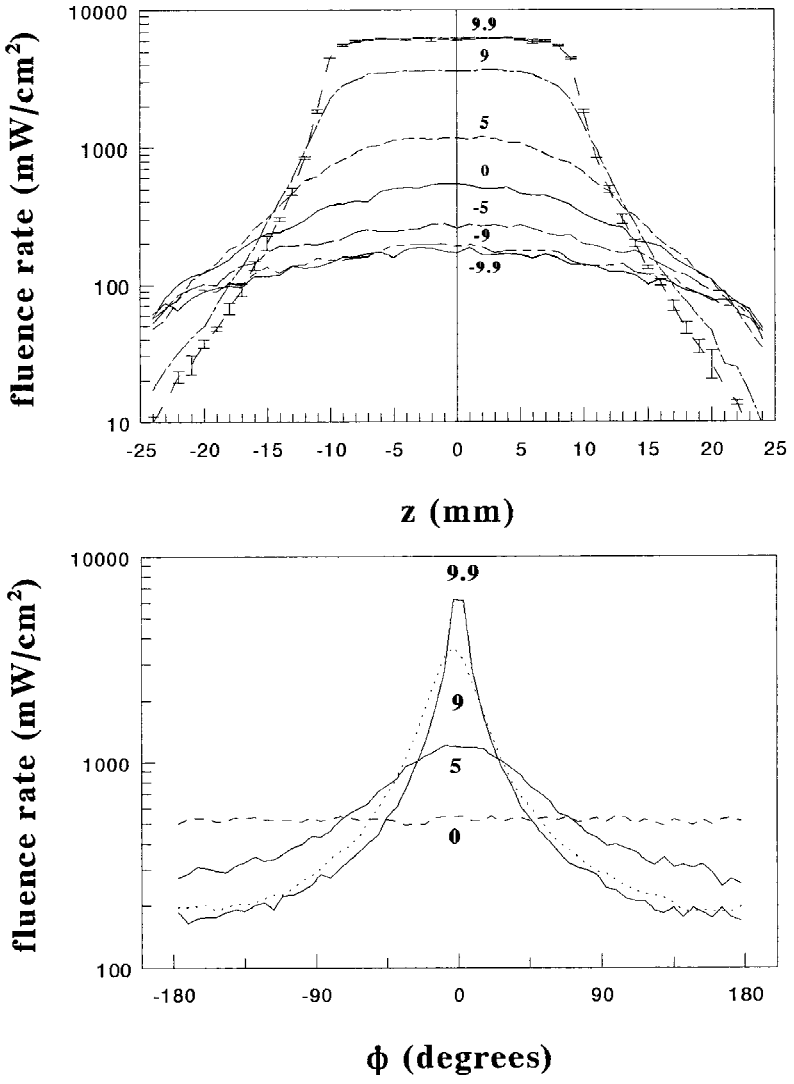

Fig. 9. Fluence rate profiles on the wall (r = 0) of a cavity (D = 2 cm) resulting from illumination with a 2 cm isotropic diffuser, optical properties for a single trachea at 630 nm (Table 1). Numbers indicate the off-axis position (mm) of the diffuser. Positive and negative numbers indicate that the diffuser is moved toward and away from the site, respectively. Top: Fluence rate profiles at $\phi = 0°$, for varying off-axis positions. Bottom: Fluence rate profiles at z = 0, for varying off-axis positions. For clarity, error bars are only indicated once in the top graph. Mean values and error bars calculated of 3 runs of 250,000 photons each.

This shows that considerable interpatient variations can occur in the applied fluence rate due to variations in optical properties as reported previously by Marijnissen et al. [11] for bladder and Hudson et al. [12] for skin at 630 nm.

The influence of blood content of the mucosa can be directly estimated from Figure 7. Changes in the order of 1 total volume percent introduce changes in the order of the average absorption at 630 nm [13], an increase in absorption of 0.15 cm^{-1} introduces a decrease of 30% in the fluence rate, and a decrease of the absorption causes even larger increases in the fluence rate. The latter may occur when vascular shutdown occurs, one of the possible effects of photodynamic therapy.

Practical Use

Several rules of thumb can be derived for use in clinical practice provided that diffusers with good characteristics are used [8]. For practical use, the β value can be assumed the same for all lumina in one patient, and then the maximum fluence rate on the wall for on-axis illumination can be calculated according to $\phi = \beta \cdot [P/(\pi LD)] \cdot \arctan(L/D)$. This relation can be used to

estimate that the maximum fluence rate increases by a factor of 2.2 when going from the trachea (D = 20 mm) to a bronchus (D = 12 mm) with a 2 cm diffuser. A protocol written to cover different areas in the bronchi should incorporate these large differences in dosimetry.

For on-axis isotropic linear diffusers, as a first-order estimate the fluence rate profile on the wall can be described as the incident fluence rate pattern enhanced by a factor β, as we observed with an ex vivo measurement in a pig trachea [10].

The geometry parameter (Q = L/D) in humans can vary between 0.25 and 7.5 because of the length of the applied diffuser (0.5–3 cm) and the diameter of the treated lumen (20–4 mm). The corresponding term correcting for the geometry (arctan(Q)) then varies from 0.24 for L = 0.5 cm and D = 2 cm (Q = 0.25) to 1.44 for L = 3 cm and D = 0.4 cm (Q = 7.5). The illumination of even smaller lumina or obstructing tumours becomes comparable to interstitial treatment and is beyond the scope of this report.

The ratio R defined by equation 4 is a measure for the homogeneity of the fluence rate profile at the bronchial wall opposite the diffuser with length L. For small Q values ($L \ll D$) this ratio approaches R = 1 and basically describes a point source geometry, in which is not possible to distinguish between center and ends of the diffuser. For large Q values ($L \gg D$), the value of R approaches 0.5. In the latter case the incident fluence rate opposite the ends of the diffuser receives contributions from one practically semi-infinite line source extending along the + or −z-axis, whereas the incident fluence rate opposite the middle of the diffuser is built up by two such semi-infinite line sources (extending along both the + and the −z-axis).

In practice, the fluence rate opposite the ends of the diffuser is 95% of the maximum in the case of the smallest Q (0.25) and 52% for the largest Q (7.5), as can be estimated with the help of eq.4. This is important to know when choosing a diffuser length for treatment of a lesion of a certain length. For treatment with a large Q, it may be wise to use a diffuser that is longer than the lesion to avoid underillumination of the edges of the tumour. The length of the diffuser can be chosen such that the incident fluence rate (eq.3) on the lesion perimeter is eg. $\geqslant$80% of the fluence rate at z = 0.

Penetration Depth

The data in Figure 6 show that for varying lumen diameter and constant optical properties, the penetration depth is a constant. The definition of penetration depth is somewhat arbitrary. If the penetration depth is defined as the depth at which the fluence rate has decreased to a certain percentage of the fluence rate at the wall, then the penetration depth is indeed constant. This, however, implies knowledge of the fluence rate at the wall of the lumen through either calculation or preferably measurement.

Another definition of penetration depth is the maximum depth at which the fluence rate exceeds a certain threshold value needed for the photosensitiser to induce tissue damage. When this definition is used, the penetration depth can be interpreted as depth of necrosis or treatment depth. With the latter definition the penetration depth increases with decreasing lumen diameter. This is not a practical definition, because it requires knowledge of the fluence rate in depth. In practical use, only a measurement at the surface is possible and therefore the first definition seems more appropriate.

Eccentric Illumination

When the diffuser is placed off-axis in the lumen, large dose variations can occur. Slight deviations from the on-axis position produce only minor variations in the fluence rate at the wall, but positions close to the wall cause an increase in dose rate at the wall of several orders of magnitude, which is very sensitive to small displacements, as we reported earlier in ex vivo measurements [1]. The fluence rate at the wall opposite the site toward which the diffuser is moved decreases to one-third of the on-axis value. A very narrow region (3 mm for total 9.9 mm eccentricity in a 2 cm diameter lumen) receives the same (within 50%) fluence, which in general is smaller than the lesion plus a margin of surrounding tissue. In case of unknown extension of premalignant tissue we advocate uniform illumination [1] as in the bladder [14] to make sure a large enough margin is treated. Therefore we strongly advise to always use an on-axis illumination if possible.

CONCLUSION

The data shown here clearly demonstrate the considerable variations in the fluence rate lev-

els and patterns as a consequence of varying geometries and optical properties. Protocols for photodynamic therapy in the bronchi should therefore be designed with special attention to the dosimetry in order to achieve reproducible results.

The relationships derived above to estimate the fluence rate should be related to an in vivo measurement of the fluence rate [2]. From this measurement a value for β can be calculated, and then the dosimetry in another lumen can be based on this β value and the knowledge of the lumen diameter and diffuser length. This, however, assumes the same optical properties in every lumen. In the case of a clearly visible lesion, an in situ measurement should be attempted. If possible, an in situ measurement of the optical properties might be performed [15] that could then be compared with an extended set of Monte Carlo simulations with varying optical properties to estimate the fluence rate distribution.

Combination of light dosimetry and a measurement of the fluorescence of the sensitiser present in the tissue [16] might prove a useful tool for optimising the treatment parameters. Monte Carlo simulations can be very useful in investigating the excitation and escape of fluorescence from the tissue.

ACKNOWLEDGMENTS

The authors thank Marleen Keijzer for supplying the basic code for the Monte Carlo simulations. The Laser Centre at the Amsterdam Medical Centre kindly provided access to the double-integrating-sphere setup.

REFERENCES

1. Murrer LHP, Marijnissen JPA, Star WM. Ex vivo light dosimetry and Monte Carlo simulations for endobronchial photodynamic therapy. Phys Med Biol 1995; 40: 1807–1817.
2. Murrer LHP, Marijnissen JPA, Baas P, van Zandwijk N, Star WM. Applicator for light delivery and in situ light dosimetry during endobronchial photodynamic therapy: First measurements in humans. Lasers Med Sci 1997; 12:258–259.
3. Marijnissen JPA, Baas P, Beek JF, van Moll JH, van Zandwijk N, Star WM. Pilot study on light dosimetry for endobronchial photodynamic therapy. Photochem Photobiol 1993; 58:92–98.
4. Saponaro S, Farina B, Murrer LHP, Pignoli B, Rizzo R, Star WM, Tomatis S, Marchesini R. Endoluminal photodynamic therapy: Influence of optical properties on light fluence in the cylindrical diffusing fibre geometry. Proc SPIE 1996; 2923:86–95.
5. Keijzer M, Pickering JW, van Gemert MJC. Laser beam diameter for port wine stain treatment. Lasers Surg Med 1991; 11:601–605.
6. Van Staveren HJ, Beek JF, Keijzer M, Star WM. Integrating sphere effect in whole bladder wall photodynamic therapy: II The influence of urine at 458, 488, 514 and 630 nm optical irradiation. Phys Med Biol 1995; 40:1307–1315.
7. Pickering JW, Prahl SA, van Wieringen N, Beek JF, van Gemert MJC. Double-integrating-sphere system for measuring the optical properties of tissue. Appl Opt 1993; 32:399–410.
8. Murrer LHP, Marijnissen JPA, Star WM. Improvements in the design of linear diffusers for photodynamic therapy. Phys Med Biol 1997; 42:1461–1464.
9. Star WM. Diffusion theory of light transport. In: Welch AJ, van Gemert MJC, eds. "Optical-Thermal Response of Laser-irradiated tissue," chap. 6, ed. New York: Plenum, 1995, pp 131–206.
10. Murrer LHP, Marijnissen JPA, Star WM. Light distribution by linear diffusing sources for photodynamic therapy. Phys Med Biol 1996; 41:951–961.
11. Marijnissen JPA, Star WM, In 't Zandt HJA, D'Hallewin MA, Baert L. In situ light dosimetry during whole bladder wall photodynamic therapy: Clinical results and experimental verification. Phys Med Biol 1993; 38:567–582.
12. Hudson EJ, Stringer MR, Cairnduff F, Ash DV, Smith MA. The optical properties of skin tumours measured during superficial photodynamic therapy. Lasers Med Sci 1994; 9:99–103.
13. Cheong WF, Prahl SA, Welch AJ. A review of optical properties of biological tissues. IEEE J Quantum Electron 1990; 26:2166–2185.
14. Marijnissen JPA, Jansen H, Star WM. Treatment system for whole bladder wall photodynamic therapy with in vivo monitoring and control of light dose rate and dose. J Urol 1989; 142:1351–1355.
15. Bays R, Wagnières G, Robert D, Braichotte D, Savary J-F, Monnier P, van den Bergh H. Clinical determination of tissue optical properties by endoscopic spatially resolved reflectometry. Appl Opt 1996; 35:1756–1766.
16. Braichotte D, Savary JF, Glanzmann T, Monnier P, Wagnières G, van den Bergh H. Optimizing light dosimetry in photodynamic therapy of the bronchi by fluorescence spectroscopy. Lasers Med Sci 1996; 11:247–254.
17. Press WH, Flannery BP, Teukolsky SA, Vetterling WT. "Numerical Recipes in Pascal: The Art of Scientific Computing." Cambridge: Cambridge University Press, 1989.
18. Lux I, Koblinger L. "Monte Carlo Particle Transport Methods: Neutron and Photon Calculations." Boca Raton: CRC Press, 1991.

APPENDIX

Construction of a Nonuniformly Distributed Random Variable

ξ is a random variable, uniformly distributed between 0 and 1 ($p_u(s) = 1$ for $0 \leqslant s \leqslant 1$, and 0 otherwise). We used Ran3 from Numerical Recipes [17].

To generate a random variable distributed according to p(s) using the uniform distribution $p_u(s)$, a function f(s) has to be found such that the following condition is obeyed [18]:

$$\int_0^{\xi} p_u(s)ds = \xi = \frac{\int_0^{s_1} p(s)ds}{\int_0^{\infty} p(s)ds} = f(s_1) \qquad (9)$$

The integral in the denominator normalizes the distribution, which is necessary because the distributions used are often obtained from (generally not normalized) measurements. The random variable s_1 is sampled through

$$s_1 = f^{-1}(\xi) \qquad (10)$$

Here we have a p(s) that is either no analytical function (measurement of output power vs. position), or a function (6^{th} degree polynomial) that has no analytical inverse function f^{-1}. Therefore, a discrete description of the functions is used, viz. a series of N x and y values (y_i, x_i). The x-values are equally spaced by Δx. Equation 9 is rewritten as:

$$\xi = \frac{\sum_{n=1}^{n1} y_n(x_n)\Delta x}{\sum_{n=1}^{N} y_n(x_n)\Delta x} = f(x_{n1}) \qquad (11)$$

The function is normalised such that $f(x_N) = 1$. For each x_{n1} value a ξ_{n1} value is calculated. The inverse function

$$x_{n1} = f^{-1}(\xi) \qquad (12)$$

is obtained by linear interpolation between the x_{n1} values paired to the two ξ_{n1} values that are closest to the ξ value generated by the uniform random number generator.